Vibronic Model for the Quantum Dynamical Study of the Competition between Bright and Charge-Transfer Excited States in Single-Strand Polynucleotides: The Adenine Dimer Case†

Roberto Improta,‡,§ Fabrizio Santoro,|| Vincenzo Barone,⊥ and Alessandro Lami*,||

Dipartimento di Chimica and INSTM, Università Federico II, Complesso Monte S. Angelo, via Cintia, I-80126 Napoli, Italy, Istituto di Biostrutture e Bioimmagini−CNR, Via Mezzocannone 16, I-80134 Napoli, Italy, Area della Ricerca, Istituto per i Processi Chimico-Fisici del Consiglio Nazionale delle Ricerche (IPCF-CNR), Via G. Moruzzi 1, I-56124 Pisa, Italy, and Scuola Normale Superiore di Pisa, Piazza dei Cavalieri 7, I-56126 Pisa, Italy

Received: July 3, 2009; Revised Manuscript Received: September 15, 2009

A simple vibronic model aimed at investigating the interplay between bright excitonic states and dark charge-transfer (CT) states in stacked adenine (Ade) nucleobases is presented. Two orbitals (the HOMO and the LUMO) for each Ade site have been included in the electronic Hamiltonian, whose parameters have been fitted to reproduce the main features of the absorption spectra of two stacked 9-methyladenine (9Me-A) molecules, computed in aqueous solution at the PCM/TD-PBE0 level. Three modes for each adenine unit have been included in the Hamiltonian, to describe the main structural changes among the different excited state minima of the adenine stacked dimer, as described at the TD-DFT level. The developed vibronic Hamiltonian (four electronic states and six nuclear coordinates) has been adopted to perform quantum dynamical calculations of a photoexcited Ade stacked dimer, utilizing the multiconfigurational time-dependent Hartree method. The obtained results indicate that the transfer between the bright excitonic state and the CT state is fast and effective.

1. Introduction

The absorption of ultraviolet (UV) light by DNA has fundamental biological implications since it can originate DNA photolesions,[1,2] like thymine dimerization that can occur from excited singlet states.[3,4] As a consequence, in the past decade many experimental and theoretical studies (too many to be exhaustively reviewed here) have been devoted to elucidate the dynamics of the excited states of DNA and of its constituents, the nucleobases.[1−29] These studies have shown that the excited state decay occurs on the subpicosecond time scale in the isolated nucleobases,[1] since both in purines[15,16] and in pyrimidines[17−22] almost barrierless paths connect the Franck−Condon (FC) region with conical intersections (CoI) with the ground electronic state (S_0). The behavior of DNA single and double strands is instead much more complex: together with ultrafast (time constant, τ, ∼0.5−1 ps) decay channels, substantial long-living components with τ in the range ∼5−200 ps exist,[1−14] and even nanosecond decays have been documented in adenine strands.[8] Furthermore, experimental and computational studies agree in predicting that the absorption process involves excited states delocalized on multiple (up to 4−6) stacked bases,[11,12] whereas the emission should stem from excited states localized on single nucleobases.[8,14] Different models have been proposed to explain the above findings, and the mechanism underlying the excited state decay within DNA single and double strands is matter of a very lively debate.[1,2,5−10,13,14] Experiments[1,2] on $(dA)_n$ and $(dT)_n$ oligomers and on $(dA)_n(dT)_n$ double strands suggest that the long-living component of the excited state decay in AT DNA can be assigned to an intrastrand excimer formed by two stacked adenine nucleobases. Actually, a long-living component (time constants in the range 10−100 ps) is present in several dinucleosides and it has been proved that its lifetime is related to the stability of the interbase charge-transfer (CT) state.[13] Experiments thus suggest that the long-living excimer has a significant CT character, and this hypothesis fully agrees with the predictions of TD-DFT computations on Ade single strands and on AT tetramer.[23−25] Alternatively, it has been suggested that the long-living component evidenced in time-resolved experiments can be attributed to a "neutral" excimer state (i.e., without any significant CT character), exhibiting a different stacking geometry with respect to typical of B-DNA.[28] In any case, independently of the character assigned to the intrastrand excimer, it seems that the excited state decay in AT DNA is ruled by the interplay between fast, "monomer-like" decay routes,[2] where a bright excited state is localized on a single nucleobase, and dark excimers,[29] with a more or less pronounced CT character, involving at least two stacked molecules.[1,2,11] Experiments indicate that the population transfer between the bright excited states and the dark excimers is very effective (it should involve ∼65% of the excited state population) and fast (it should occur on a subpicosecond time scale).[1] It would thus be very useful to thoroughly characterize this transfer by means of quantum dynamical (QD) calculations, to verify if its features are consistent with the experimental indications. Furthermore, such a study should include a very large number of nucleobases since, as we have anticipated above, the spectroscopic state is delocalized on several bases. These requirements clearly point out the necessity of developing suitable simplified models, since a complete QD simulation of a system composed of several nucleobases is computationally too expensive. Such models

† Part of the "Vincenzo Aquilanti Festschrift".

* Corresponding author. E-mail: lami@ipcf.cnr.it.
‡ Università Federico II.
§ Istituto di Biostrutture e Bioimmagini−CNR.
|| Istituto per i Processi Chimico-Fisici del Consiglio Nazionale delle Ricerche (IPCF-CNR).
⊥ Scuola Normale Superiore di Pisa.

10.1021/jp906278t
Published on Web 10/12/2009

should be able to reproduce, at least semiquantitatively, the results of accurate quantum-mechanical (QM) calculations.

As a first step in this direction, moving along lines similar to those proposed by Bittner,[30,31] in the present paper we build a minimal electronic model involving only the HOMO and LUMO of each adenine unit. Ab initio results show, however, that the coupling between electronic and nuclear motion plays an important role and must be taken into account to get a realistic picture of the fate of the electronic energy gained by polynucleotides through photon absorption in the UV range. The purely electronic model is then improved to include the most relevant vibrational coordinates, and it is applied to the study of nonadiabatic dynamics of a photoexcited stacked adenine dimer by a MCTDH (multiconfigurational time-dependent hartree) approach. As far as we know, this is the first attempt in this direction concerning polynucleotides. A paper that is quite parallel to the present one and that also contains interesting ideas on the way one may include more vibrational degrees of freedom in a vibronic model is that of Tamura et al.[32] concerning the role played by phonon coupling in the ultrafast exciton decay observed in semiconducting polymers.

While the electronic model involving only HOMO and LUMO of the single units can be easily generalized to the study of longer strands, the inclusion of vibronic coupling can hardly be extended to more than three or four units. For that reason we plan to use the present results for the dimer (as well as the forthcoming ones for the trimer) to investigate the excitation dynamics in longer chains by a density matrix approach, in which the electronic−nuclear coupling is included under the form of dephasing as well as decay times of purely electronic density matrix elements.

We further notice that, while in the present work, the parameters of the model have been adjusted to reproduce the absorption spectra of the stacked adenine dimer computed in aqueous solution at the PCM/TD-PBE0 level,[21,22] they can be easily adapted to other computational approaches. In the results section we also report a test of the dependence of our prediction on the values of the parameter ruling the energy order of excitonic and charge-transfer states.

2. Theoretical Model

2.1. Electronic Model Hamiltonian. Let us start from the electronic model Hamiltonian, which, as anticipated, includes only the HOMO and LUMO of each unit and let us consider the general case of an oligomer composed of N identical stacked units arranged as in the B DNA. In the ground state the HOMOs of the bases of the chain are all doubly occupied. We assume that low lying excited states can be described within the manifold obtained moving a single electron from a HOMO to a LUMO. Introducing second quantized operators for holes (h) and electrons (e), and assuming as vacuum the state ($|\mathrm{vac}\rangle$) in which all HOMOs are doubly occupied (i.e., no holes in the HOMOs and no electrons in the LUMOs) the electronic model Hamiltonian is written as

$$H_{\mathrm{el}} = \sum_{j=1,N-1;\sigma=\uparrow,\downarrow} [t_{\mathrm{h}}(h^{+}_{j+1,\sigma}h_{j,\sigma}+\mathrm{hc}) + t_{\mathrm{e}}(e^{+}_{j+1,\sigma}e_{j,\sigma}+\mathrm{hc})] + \sum_{j=1,N-1;k=j,N} n^{\mathrm{h}}_{j}n^{\mathrm{e}}_{k}R_{jk} \quad (1)$$

where

$$n^{h}_{j} = h^{+}_{j\uparrow}h_{j\uparrow} + h^{+}_{j\downarrow}h_{j\downarrow};\ n^{e}_{j} = e^{+}_{j\uparrow}e_{j\uparrow} + e^{+}_{j\downarrow}e_{j\downarrow}$$

The parameters in eq 1 are simply hopping terms for holes and electrons (t_{h} and t_{e}, respectively) and an electrostatic term R (depending on the electron−hole distance), which determines the relative stability of localized exciton states (those with $j = k$) and CT states, and will be determined to reproduce accurate ab initio computations. In the following we will be concerned with the dimer case for which we will take $R_{11} = R_{22} = 0$ while $R_{12} = R_{21} = R$. Notice that to investigate dynamics neither the HOMO and LUMO orbital energies nor the Hubbard repulsion U between two electrons in the same HOMO are required. These parameters, in fact, play simply the role of shifting the energy of the excited manifold as a whole.

In the following we will also need to shift to a matrix representation of the electronic degree of freedom. We then introduce the singlet basis set:

$$|j, k\rangle = \frac{1}{\sqrt{2}}(h^{+}_{j\uparrow}e^{+}_{k\downarrow} + h^{+}_{j\downarrow}e^{+}_{k\uparrow})|\mathrm{vac}\rangle \quad (2)$$

where $|j, k\rangle$ is the singlet state obtained creating a hole at site j and an electron at site k (i.e., moving an electron from the HOMO at site j to the LUMO at site k). Notice that the first index in the ket gives the position of the hole and the second one that of the electron. As previously mentioned, when $j = k$, one recovers a localized excitonic state.

The above picture is essentially diabatic, being based on states in which electrons (holes) are localized, i.e., assigned to given sites. The hopping terms ensure mobility of electrons and holes leading to adiabatic (delocalized) states.

2.2. Vibronic Effects. In this section we complete our model introducing the nuclear coordinates. In the next section we will show that on the basis of a TD-DFT analysis for the adenine dimer procedure one may identify three localized modes for each adenine unit, which enter predominantly in describing the different minima of the potential energy surfaces (PES) for the excited states involved. These modes are named $Q_{k\alpha}$ where the first index (latin) identifies the kind of vibration one is dealing with, while the second one (greek) indicates the unit where it is localized ($\alpha = 1, 2$ for the dimer). These modes are considered here harmonic and their frequencies are taken as constant, i.e., identical for the adenine in the ground, cationic, anionic or excited state (A, A^{+}, A^{-}, A*). The equilibrium position, however, depends on the nature of the localized electronic state, and it is indicated by $Q^{0}_{k\alpha}(ij)$ (where the couple of indexes in parentheses specify the electronic state, according to the notation introduced in eq 2). Taking as an example the trimer, Q_{13} is the first vibration of the third unit and $Q^{0}_{13}(12)$ is the equilibrium position of such mode in the adenine ground state, since $|1, 2\rangle \equiv |A^{+}, A^{-}, A\rangle$. Using dimensionless coordinates, the vibronic Hamiltonian is then

$$H_{\mathrm{vib}} = H_{\mathrm{el}} + \sum_{i,j} [|i,j\rangle\langle i,j| \sum_{\nu,\alpha} (V_{\nu\alpha}(ij) + T_{\nu\alpha})] \quad (3)$$

where

$$V_{\nu\alpha}(ij) = \frac{1}{2}\omega_{\nu}(Q_{\nu,\alpha} - Q^{0}_{\nu,\alpha}(ij))^{2} \quad (4)$$

and

$$T_{v\alpha} = -\frac{1}{2}\omega_v \frac{\partial^2}{\partial Q^2_{v\alpha}} \quad (5)$$

Since in the following we will focus on the dimer case, we rewrite eqs 1 and 2 in an expanded but more transparent form (we indicate by q the coordinates on the first adenine unit and by Q those on the second one):

$$H_{el} = (|A^+A^-\rangle\langle A^+A^-|R + hc) + (|A^*A\rangle\langle A^+A^-|t_e + hc) + (|A^*A\rangle\langle A^-A^+|t_h + hc) \quad (6)$$

$$\begin{aligned} H_{vib} = H_{el} &+ |A^*A\rangle\langle A^*A|\left\{\frac{1}{2}\sum_v \omega_v\left[(q_v - q^0_{vA^*})^2 - \frac{\partial^2}{\partial q_v^2}\right] + \frac{1}{2}\sum_v \omega_v\left[(Q_v - Q^0_{vA})^2 - \frac{\partial^2}{\partial Q_v^2}\right]\right\} + \\ &|AA^*\rangle\langle AA^*|\left\{\frac{1}{2}\sum_v \omega_v\left[(q_v - q^0_{vA})^2 - \frac{\partial^2}{\partial q_v^2}\right] + \frac{1}{2}\sum_v \omega_v\left[(Q_v - Q^0_{vA^*})^2 - \frac{\partial^2}{\partial Q_v^2}\right]\right\} + \\ &|A^+A^-\rangle\langle A^+A^-|\left\{\frac{1}{2}\sum_v \omega_v\left[(q_v - q^0_{vA^+})^2 - \frac{\partial^2}{\partial q_v^2}\right] + \frac{1}{2}\sum_v \omega_v\left[(Q_v - Q^0_{vA^-})^2 - \frac{\partial^2}{\partial Q_v^2}\right]\right\} + \\ &|A^-A^+\rangle\langle A^-A^+|\left\{\frac{1}{2}\sum_v \omega_v\left[(q_v - q^0_{vA^-})^2 - \frac{\partial^2}{\partial q_v^2}\right] + \frac{1}{2}\sum_v \omega_v\left[(Q_v - Q^0_{vA^+})^2 - \frac{\partial^2}{\partial Q_v^2}\right]\right\} \end{aligned} \quad (7)$$

3. Results

3.1. Data from TD-DFT Calculations. All the data needed for our vibronic models have been obtained by DFT and TD-DFT[33,34] calculations using the PBE0 exchange-correlation functional.[35]

Geometry optimizations in solution were performed at the PCM/PBE0/6-31G(d) level for the ground electronic state S_0 while excited state geometries were optimized at the PCM/TD-PBE0/6-31G(d) level, based on the linear response (LR) theory.[36] This approach has already been successfully applied for pyrimidine and purine excited states.[16−25] It provides vibrationally resolved spectra in the condensed phase in agreement with experiment.[37,38] All the computed vibrational frequencies in the minima of the ground and excited states are positive.

The LR-PCM/TD-PBE0 results have been further checked by using CAM-B3LYP,[39] M05-2X,[40] and LC-ωPBE[41] density functionals, and using the state-specific (SS) implementation of PCM/TD-DFT.[42,43] Bulk solvent effects on the electronic states have been included by using the polarizable continuum model (PCM).[44]

All the calculations have been performed by using a development version of the Gaussian03 program.[43]

The electronic parameters of our model have been obtained by fitting the absorption spectrum computed in ref 23 by TD-DFT calculations at the vertical ground state equilibrium geometry, which is reported in Figure 1. As discussed in detail in refs 23−25, the computed spectrum fully reproduces all the main features of the experimental absorption spectrum of polyAde single strand,[8,14] when compared to that of adenine monophosphate: (i) a slight blue shift of the maximum of the absorption, (ii) a slight red shift of the low-energy side, and (iii) a significant decrease in oscillator strength. Four electronic transitions involve the frontier orbitals (HOMO and LUMO) of the stacked 9Me-A molecules, and two of these transitions are bright. These latter, within the framework of the simple excitonic model applied to an H-type dimer, are related to the bright excited states of the A nucleobases. Due to the excitonic coupling, the two bright transitions are no more degenerate and exhibit different intensities: one is bright and intense, and the other one is bright but weak. It is also important to remember that the frontier orbitals and the corresponding bright electronic transitions are delocalized over the two 9Me-A bases. In the red part of the spectrum two electronic transitions with partial CT character are present. If the frontier molecular orbitals were localized on each nucleobase, they would correspond to the excitation on an electron from the HOMO of a base to the LUMO of its stacked partner.

It must be taken into account that that TD-DFT calculations employing "standard" functionals have shown significant failures in the treatment of CT transitions.[26,27,33] Furthermore, more sophisticated PCM implementations, such as the recently developed state-specific (SS) PCM/TD-DFT method,[42,43] are necessary to correctly include the solvent effect on CT transitions. We have therefore re-evaluated the relative energy of the lowest energy excited states in the adenine single strand, by comparing the results obtained at the LR-PCM/TD-PBE0 level with those provided by other density functionals such as CAM-B3LYP,[39] M052X,[40] and LC-ωPBE,[41] which are more suitable to the study of CT transitions in stacked systems, using SS-PCM method[40,41] for including solvent effect.[22] This analysis has shown that, as expected, PBE0 overestimates the stability of CT transitions but, at the same time, LR-PCM underestimates the solvation energy of the CT states.[24] These two errors tend to cancel each other and the performed analysis[24] has confirmed the results of our previous investigations,[23] indicating that CT states are slightly more stable than the most intense bright excited states of the adenine dimer. This prediction has been questioned by another very recent computational study employing LC-ωPBE and LC-ωPBEh functionals (the low-energy tail of the CT tail overlaps with the high-energy side of the bright transition)[27] and on the ground of CASPT2 calculations.[28] In conclusion, a lively debate still exists on the energy ordering of these states and it is therefore worth highlighting that the model we have developed in the present paper is pretty general and that, by tuning its parameters, it is possible to simulate also a different energy ordering between the bright and the CT states.

In refs 23 and 24 we performed a detailed TD-DFT analysis of the adenine stacked dimer in water. Geometry optimizations of the bright excited states lead to a structure where the excitation is localized on a single A monomer $|AA^*\rangle$.[23] Optimization of the lowest energy state in the FC region led to a charge-transfer state (amount of transfer >0.8) where one of the two A (the donor) assumes the typical geometry of the cation A^+ while the other shows the structure of the anion A^- .

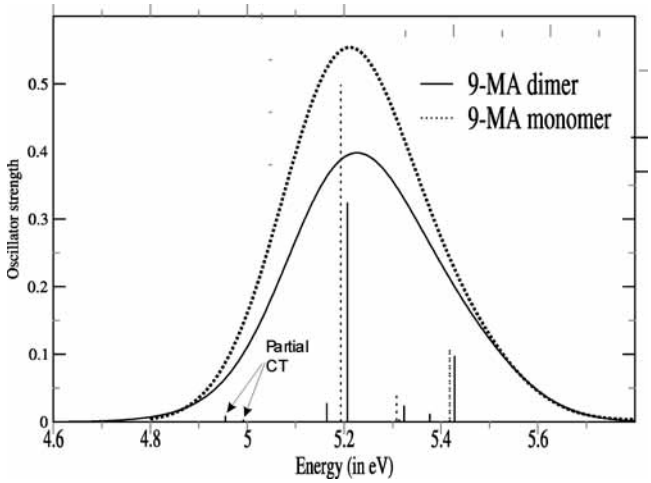

Figure 1. Comparison between the absorption spectrum computed for the 9Me-A stacked dimer and the 9Me-A monomer at the PCM/TD-PBE0/6-31G(d) level by Improta et al.[21]

Before discussing how the above results have been used to select the vibrational degrees of freedom to include in our model, it is important to highlight that they provide a picture fully consistent with the experimental indications. Indeed, the results obtained on nucleosides[13] and the similarity of the behavior exhibited by the long-living excimers within single and double strands[5] find the most natural explanation in our prediction that the lowest energy excited state of Ade single strand has a substantial CT character.[23−25] Furthermore, fluorescence up-conversion experiments indicate that the emission should stem from excited states localized on a single nucleobase,[8,14] and its features are very similar to those of the isolated adenine.[14]

The localized states predicted by PCM/TD-PBE0 excited state geometry optimizations are pretty close to our diabatic states $|AA^*\rangle$ and $|A^+A^-\rangle$, and clearly each of them has its symmetric counterpart ($|A^*A\rangle$ and $|A^-A^+\rangle$, respectively), even if residual coupling can make them slightly different. The equilibrium geometries of our fully localized diabatic states can be easily guessed by determining, in aqueous solution, the minimum ground state structures of the neutral (A^0), cation (A^+), and anion (A^-) adenine monomer and the minimum structure of the HOMO → LUMO excited adenine ($A^{\pi\pi^*}$). These structures were obtained at the PCM//PBE0/6-31G(d) level for ground state species and at the PCM//TD-PBE0/6-31G(d) level for the $A^{\pi\pi^*}$ excited state.

We chose to adopt the normal modes of the ground state A^0 as a set of coordinates to describe nuclear dynamics. These coordinates were obtained by a standard PCM//PBE0/6-31G(d) harmonic analysis around the A^0 equilibrium geometry. With the aim to restrict our investigation ultrafast dynamics, the intermonomer coordinates (distance and orientation) were taken frozen at the B-DNA structure. Analogously, we performed the optimization by imposing the constraint of planarity, since out-of-plane motions are expected to be slower (and, being not totally symmetric, at the FC planar point the driving force to remove the planarity is zero).

Here we selected three coordinates per each adenine unit (i.e., six coordinates). These represent combined motions of the atoms of the adenine ring (see Table 1). In analogy with a procedure we have already followed to study uracil excited state dynamics,[44] their combinations allow us to move from the FC point (i.e., the equilibrium geometry of adenine A^0) to the equilibrium geometries of the cation A^+, the anion A^- and the $\pi\pi^*$ state $A^{\pi\pi^*}$, which are involved in all the relevant minima of the diabatic excited states of the dimer.

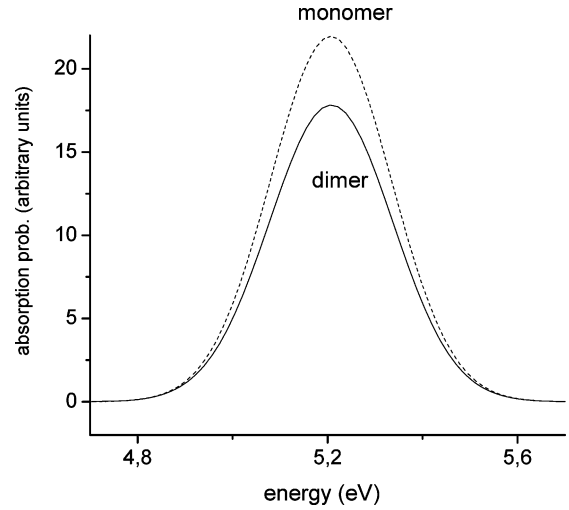

Figure 2. Absorption spectrum from the purely electronic Hamiltonian, eq 1 with the parameters reported in the text. The three lines of Appendix A have been transformed to Gaussians with a fwhm = 0.3 eV. The spectrum of two independent monomers is also reported for comparison. The decrease of the integrated oscillator strength in passing from the dimer to two independent monomers is entirely due to a geometric effect (see Appendix A).

TABLE 1: For Adenine in Water, the Main Dimensionless Displacements of the S_0 Normal Modes (Together with Their Harmonic Frequencies), between the S_0 Equilibrium Geometry of Adenine A^0 and the Equilibrium Geometries of the Cation A^+, the Anion A^-, and the $\pi\pi^*$ State $A^{\pi\pi^*}$ (HOMO−LUMO Excitation) (PCM//PBE0/6-31G(d) and PCM//TD-PBE0/6-31G(d) Calculations)

	ω (cm^{-1})	A^0	A^+	A^-	$A^{\pi\pi^*}$
Q_{16}	740.29	0	−0.418	0.934	0.422
Q_{38}	1578.61	0	−0.734	−0.334	−0.882
Q_{40}	1659.28	0	0.372	0.245	0.768

3.2. Parameters for the vibronic Hamiltonian. The parameters for the vibronic model Hamiltonian, eq 3, have been determined by having in mind the TD-DFT results presented in section 3.1. First let us consider the electronic part H_{el} and notice that the electronic model Hamiltonian in eq 1 gives rise to three absorption lines whose position and height can be easily evaluated as a function of t_e, t_h, and R, as shown in Appendix A. The above spectrum must be compared with the PCM-TDDFT one in Figure 1. The latter, as expected, contains many more lines with respect to the three lines resulting from our minimal model Hamiltonian. Furthermore, the comparison with TDDFT assignments (see ref 21) is not immediate since they are based on delocalized molecular orbitals, while here we have to do with localized valence bond configurations (Slater determinants). Assuming a negative value for both t_e and t_h the most intense spectral line (on the blue side) is due to a transition between the ground state and a linear symmetric combination of $|E_+\rangle$ and $|CT_+\rangle$. As one can easily check, the $|E_+\rangle$ state (the bright one) is the VB translation of the H → L+1 + H−1→ L transition, in agreement with the results in ref 21 (Table 1). In Figure 2 we report the spectrum obtained from eq 1 with $t_e = t_h = -100\ cm^{-1}$ and $R = -300\ cm^{-1}$. This choice of parameters warranties the best agreement with the TDDFT ones given in Figure 1. We notice that the mobilities of electrons and holes are taken to be identical and low, which agrees with previous estimates[28] while R is also small and negative, which means that CT states are slightly more stable than excitonic states. This relative order of stability is the one resulting from our PCM/

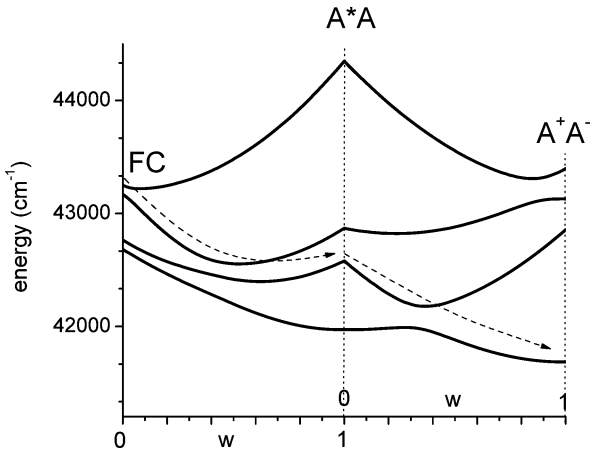

Figure 3. Potential energy profiles of the four adiabatic states of our adenine dimer model for a selected path going (from left to right) from the Franck−Condon region (in which the electronic excitation is shared between the two adenine units) to the minimum of the diabatic state in which excitation is localized on the first adenine and then to the minimum of the charge separated state A^+A^-. The variable w varying between 0 and 1 is a linear interpolation parameter (see text). The dashed line shows a possible path leading to electronic energy dissipation due to nonadiabatic dynamics at various avoided crossings.

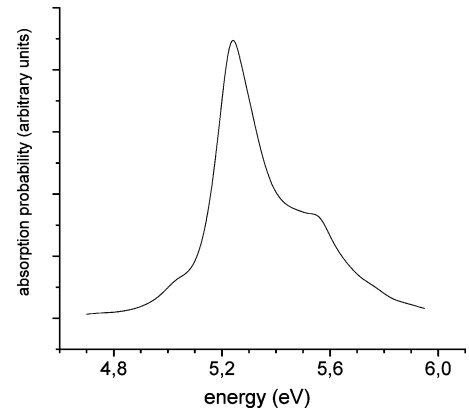

Figure 4. Absorption spectrum of the adenine dimer, as described by the vibronic Hamiltonian, eq 6. It has been computed from the Fourier transform of the autocorrelation function obtained propagating a doorway state. The latter is a delocalized exciton state obtained mixing the two localized exciton states with equal weight, which means that the light electric field is assumed to form identical angles with the transition dipole of both adenine units (see Appendix B). Since, as mentioned in the text, the model Hamiltonian does not carry information on the energy gap between the ground state and the excited manifold of states containing one electron and one hole, we have simply translated it along the energy axis to match the maximum with TDDFT calculations.

TD-DFT calculations. The small value of hopping parameters is necessary to avoid a too pronounced shoulder on the red site of the spectrum.

The vibronic part of the model Hamiltonian is then built up by including the relevant modes in Table 1 describing combined motions of the atoms of the adenine rings.

3.3. Adiabatic States. An analysis of adiabatic states can be easily performed starting from the Hamiltonian in eq 7 and neglecting the nuclear kinetic energy terms. The eigenvalues give adiabatic PES as a function of the nuclear coordinates included in the model. Notice that due to the fact that the hopping parameters t_e and t_h do not depend on the nuclear coordinates (and therefore never vanish), our model does not describe conical intersections but actually avoided crossings.

Due to the large number of coordinates involved, we decided to select a few special trajectories connecting the minima of diabatic states (which, due to the small hopping terms, essentially coincide with the minima of adiabatic states, as we will see). These are function of a single parameter w ranging from 0 to 1. As an example, the trajectory from the Franck−Condon region to the minimum of $|A^* A\rangle$ is described by

$$\mathbf{R}_{FC\rightarrow A^*A}(w) = w\mathbf{R}^0_{A^*A}$$

while the one from the minimum of $|A^* A\rangle$ to that of $|A^+A^-\rangle$ is

$$\mathbf{R}_{A^*A\rightarrow A^+A^-}(w) = w(\mathbf{R}^0_{A^+A^-} - \mathbf{R}^0_{A^*A}) + \mathbf{R}^0_{A^*A}$$

Here, for example, $\mathbf{R}^0_{A^*A} = (q^0_1, q^0_2, q^0_3, Q^0_1, Q^0_2, Q^0_3)_{A^*A}$. The potential energy profiles of all the adiabatic states along the selected paths (i.e., as a function of w) are shown in Figure 3.

Inspection of Figure 3 strongly suggests that it is practically impossible to have an idea of the nuclear dynamics by just looking at the adiabatic PES, due to the many avoided crossing regions. For example, one may imagine that a way to dissipate electronic energy is the one illustrated with a dotted line in Figure. 3, leading from the FC region (on the highest excited state; see Figure 4) to the localized exciton state $|A^*A\rangle$ (with a minimal energy barrier) and then to the $|A^+A^-\rangle$ minimum on the right. It is, however, clear that only a multidimensional wavepacket propagation can give a satisfactory answer to the problem of how the photoexcited population distributes among diabatic electronic states as a function of time.

3.4. Quantum Dynamical Calculations. As we discussed in the previous section, the complexity of the relevant PES make impossible an understanding of the nonadiabatic dynamics of the system on the grounds of their mere inspection, and a true dynamical simulation is mandatory. The propagation of a 6-dimension wavepacket that can jump among four coupled electronic states is a challenging task. The most popular direct methods for solving the time-dependent Schroedinger equation can hardly be applied due to their exponential scaling law as a function of the number of coordinates. As an example, if a basis set of 30 harmonic states is chosen for each oscillator in a given electronic state, one should manage $4 \times 30^6 = 2916$ million states. A similar problem arises if one works on a grid of points. The many-body problem can be, however, safely reduced to a tractable number of dimensions using the variational approach in a more subtle way, i.e., expanding the wave function in a certain number of products of time-dependent single-particle wave functions (SPWs). This is the multiconfigurational time-dependent Hartree (MCTDH) method first applied by Cederbaum and co-workers.[45−47] Here both the coefficients weighting each Hartree configuration and the various SPWs by which the latter is built up are determined on the basis of the time-dependent Dirac−Frenkel variational theorem. The whole procedure and the basic equations have been reported in various papers and discussed in detail in ref 47. Here we only briefly sketch the way the MCTDH approach has been applied to the specific problem under investigation.

For our adenine dimer model, eq 7, the state to be determined as a function of time is written as

$$|\psi(t)\rangle = \sum_{\alpha,\mathbf{s},\mathbf{S}} c_{\alpha,\mathbf{s},\mathbf{S}}(t)|\alpha\rangle G_{\alpha,\mathbf{s},\mathbf{S}}(\mathbf{q},\mathbf{Q};t)$$
$$G_{\alpha,\mathbf{s},\mathbf{S}}(\mathbf{q},\mathbf{Q};t) = g_{\alpha,s_1}(q_1)\, g_{\alpha,s_2}(q_2)\, g_{\alpha,s3}(q_3)\, G_{\alpha,S_1}(Q_1)\, G_{\alpha,S_2}(Q_2)\, G_{\alpha,S3}(Q_3) \quad (8)$$

where $\mathbf{s} = (s_1, s_2, s_3)$,$\mathbf{S} = (S_1, S_2, S_3)$ are indexes for the SPWs g and G, attached to sites 1 and 2, respectively, and $|\alpha\rangle$ are the electronic states (four in our dimer model). Taking 2 SPWs for each vibrational mode (i.e.: $s_1 = 1, 2$; $s_2 = 1, 2, ...$; $S_3 = 1, 2$) gives 64 SPWs for each electronic state. Hence a single run of the code results in the time propagation of 256 coefficients $c_{\alpha,\mathbf{s},\mathbf{S}}(t)$ and 256 SPWs, represented on a grid of 64 points. The convergence of results has been checked with respect to the time step for the integration, the number of configurations and the number of grid points. The energy conservation has been also constantly monitored.

As the initial state, we take the one obtained through a vertical excitation from the ground state to the various bright excited states (weighted according to the matrix elements of $\mathbf{E}\boldsymbol{\mu}$ where $\mathbf{E}$ is the electric field and $\boldsymbol{\mu}$ is the electric dipole operator). As discussed in Appendix B, since the two oscillator-strength carrying states (the exciton states) have nonparallel transition moments, it is not possible in principle to reduce the problem of the random orientation of the molecule with respect to the light electric field by an a posteriori angular average. The vertically excited doorway state, in fact, does not simply depend on the geometry through a multiplicative factor. The above means that one should perform many propagations. This could be in principle avoided, for the present case, taking advantage from the symmetry of the system, but, unfortunately, this way is not practicable since, as shown in Appendix B, the results depend on the relative phase of wavepackets located on different PES and the propagation method cannot warrantee a sufficient numerical accuracy for such quantity (while it is fully reliable for the shape of the wavepackets on the four diabatic surfaces as well as for the populations).

We will then limit our illustration to the results of our calculations for the case in which the field forms identical angles with the two transition moments. It is worth recalling that for parallel transition moments this would be the exact result. Since the angle is not large (36°), one can expect that the angular average would not significantly modify the results concerning the absorption spectrum and the diabatic state populations. The former, computed by the Fourier transforming the autocorrelation function, is reported in Figure 4.

The computed populations for the case in which the two exciton states have equal weight (i.e., the electric field forms identical angles with the two transition moments) are shown in Figure 5 (full lines). The purely excitonic initial state (fully delocalized) gains a considerable CT component in a few tens of femtoseconds. This is an interesting result, since it is fully consistent with the experimental indications. Indeed, time-resolved transient-absorption studies predict that the formation of the CT state is extremely fast and effective: it involves almost 65% of the bright excited state population, and the population transfer is completed within 1 ps after the excitation.[1] Inspection of Figure 5 shows that already after 50 fs ∼40% of the excited state population has been transferred to the CT state.

This process is, however, highly oscillatory with some evidence of a slow damping. This reversibility may be attributed, at least in part, to the small number of vibrational modes included in our model. This is particularly important for CT states in which we expect that a significant relaxation effect

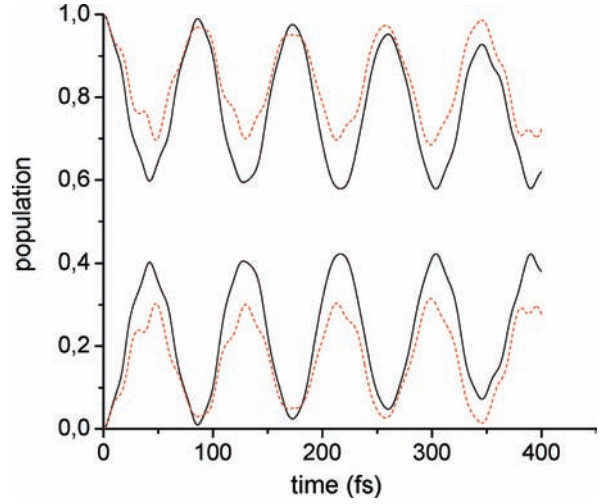

Figure 5. (Full lines) populations of the exciton and CT states computed by the MCTDH approach. The initial excited state is the symmetric linear combination of the two localized excited states, each one arising from the vertical excitation of the ground state wavepacket up to the (localized) exciton state. The parameters used for the Hamiltonian are those discussed in the text. (Dashed lines) same as above with the only difference concerning the sign of R (i.e., here $R = 300\ \mathrm{cm}^{-1}$).

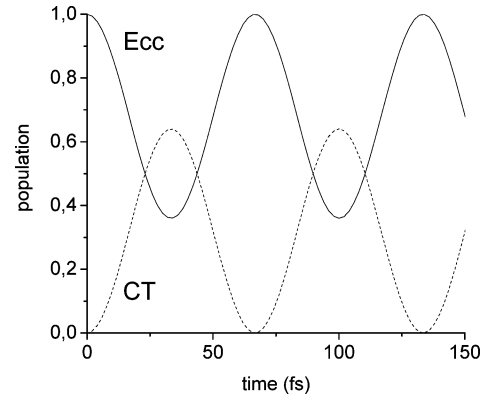

Figure 6. Populations of the localized exciton and of the CT states computed according to the pure electronic Hamiltonian in eq 2.

may come from the solvent rearrangement. In fact, while in building up the electronic Hamiltonian, eq 2, we have utilized TDDFT calculations by taking into account the rapid (electronic) component of solvation, the effect of solute−solvent modes, exhibiting periods in the femtosecond range, has been completely neglected.[42] In spite of the above limitations the results of Figure 5 are significant since they clearly document a relevant role played by vibronic effects, which are completely absent in previous models for DNA, where the focus is on the electronic band structure. To appreciate this fact, it is also useful to look at the results obtained by the purely electronic Hamiltonian, eq 2, shown in Figure 4. A perusal of the two figures shows that, as expected, the inclusion of vibronic effects reduces the amount of population transfer between exciton and CT states, while increasing the period of recurrence. In fact, the population of the CT states reaches its maximum already after ∼30 fs, and it involves more than 60% of the total excited state population.

It is also interesting to investigate the sensibility of the dynamics to the order of stability of localized exciton and CT states which, as discussed in section 3.1, is a debated point. To this purpose, we have also performed calculations by changing the sign of the parameter R. The results, shown in the dashed curves of Figure 5, reproduce the general behavior of the

previous case, with oscillations having a period of about 100 fs. One may also observe that from one side the maximum amount of population transfer from exciton states to CT states is reduced to about 30% and from the other side the population recovered after each period is also reduced. One may conclude that, within the small energy differences considered here, the relative stability of localized exciton and CT states does not dramatically change the dynamical behavior of populations.

4. Conclusions

In this contribution we have presented a simple vibronic model aimed to investigate the interplay between bright excitonic states and dark charge-transfer states in stacked single strand nucleobases, with special reference to the Ade stacked dimer in B-DNA conformation. To make the model as simple as possible, both reducing its computational cost and allowing a better understanding of the main features of the process under investigation, only two MO's (the HOMO and the LUMO) for each Ade site have been included in the electronic Hamiltonian. This latter has a limited number of parameters (the intersite hopping parameters for electron and holes and the electron hole interaction R), which have been fitted to reproduce the main features of the absorption spectrum of two stacked 9Me-A molecules, computed in aqueous solution at the PCM/TD-PBE0 level.[21] The vibronic part of the Hamiltonian has been also modeled on the ground of the results of our previous studies of Ade single strand, which shows that the excited state dynamics is ruled by the interplay between a bright excitonic state and a CT state. The former is delocalized on two Ade monomers in the absorption process, whereas the emission process is localized on a single nucleobase $|AA^*\rangle$. The latter involves the transfer of an electron between the two stacked 9Me-Ade molecules (A^+,A^-), and it is predicted to represent the absolute excited state minimum. Three modes for each adenine unit have been included in the Hamiltonian, whose different equilibrium positions are able to describe the different minima of the PES for the excited electronic states involved (A, A^+, A^-, A^*). The resulting vibronic Hamiltonian has then been used in MCTDH quantum dynamical calculations of the Ade stacked dimer. Although the limited number of degrees of freedom considered does not allow any irreversible process, the results of the QD calculations are in line with the evidence derived from time-resolved transient-absorption experiments,[3] indicating that the transfer between the bright excitonic state and the CT state is fast and effective (after 50 fs the excited state population transferred to CT states is ~40%). It is also worth mentioning that the relative stability of localized exciton and CT states (i.e., the sign of R in the model Hamiltonian) does not significantly change the main conclusions of the present investigation. Furthermore, the QD results allow appreciating the role played by the vibrational degrees of freedom, which significantly modulate the rate of the process. As previously mentioned, the small number of modes included (three for each Ade units) prevents us from having a precise picture of the time behavior after a few hundred femtoseconds. To extend this limit, we are currently evaluating the possibility of making recourse to a hierarchical model for including more vibrational degrees of freedom, as suggested by Tamura et al.[30]

On the balance, the results of this study provide encouraging indications on the suitability of vibronic model Hamiltonians for the study of the excited state dynamics in DNA single and double strands. It is important to highlight, in fact, that although our model has been parametrized on the results of PCM/TD-PBE0 calculations on the stacked Ade dimer, it could be easily adapted to reproduce the indications of other quantum mechanical approaches.

Acknowledgment. We dedicate the paper to the memory of Professor Giuseppe Del Re, a well-known theoretical chemist who died in February 2009. Thanks to his tireless and inspired activity in promoting informal contacts among scientists, some of us had the opportunity to meet Vincenzo Aquilanti and to have with him long and illuminating discussions. We thank CNR-VILLAGE for computational resources.

Appendix A

Let us compute the absorption lines obtained from the purely electronic Hamiltonian, eq 6. The latter can be represented as the following 4×4 matrix using the basis set ($|A^*A\rangle$, $|A^+A^-\rangle$, $|A^-A^+\rangle$, $|A\,A^*\rangle$):

$$\begin{pmatrix} 0 & t_e & t_h & 0 \\ t_e & R & 0 & t_h \\ t_h & 0 & R & t_e \\ 0 & t_h & t_e & 0 \end{pmatrix} \tag{A1}$$

To exploit symmetry, we resort to normalized symmetric and antisymmetric combinations of exciton states and charge-transfer states. In the new basis set ($|E_+\rangle$, $|CT_+\rangle$, $|E_-\rangle$, $|CT_-\rangle$)

Equation A1 becomes

$$\begin{pmatrix} 0 & t_e + t_h & 0 & 0 \\ t_e + t_h & R & 0 & 0 \\ 0 & 0 & 0 & t_e - t_h \\ 0 & 0 & t_e - t_h & R \end{pmatrix} \tag{A2}$$

Let us now take the dimer as fixed in a space framework, with $\boldsymbol{\mu_1}$ (the transition dipole of the first adenine unit) oriented along the z axis and $\boldsymbol{\mu_2}$ in the xz plane, forming with the first an angle $\alpha = 36°$ (like in B-DNA). The electric field **E** oscillates along the direction (θ, φ). From the diagonalization of the block matrix (A2) one has three lines whose positions and weights are respectively

$$\begin{aligned} E_1 &= R/2 - \sqrt{(R/2)^2 + (t_e + t_h)^2} \quad I_1 = Z_+ \cos^2(\chi_+) \\ E_2 &= R/2 + \sqrt{(R/2)^2 + (t_e + t_h)^2} \quad I_2 = Z_+ \sin^2(\chi_+) \\ E_3 &= R/2 - \sqrt{(R/2)^2 + (t_e + t_h)^2} \quad I_3 = Z_- \cos^2(\chi_-) \\ E_4 &= R/2 + \sqrt{(R/2)^2 + (t_e + t_h)^2} \quad I_3 = Z_- \sin^2(\chi_-) \end{aligned} \tag{A3}$$

$$Z_\pm = \frac{(E_0\mu)^2}{2}(\cos(\theta) \pm \sin(\beta)\sin(\theta)\cos(\phi) + \cos(\beta)\cos(\theta))^2$$

and

$$\chi_\pm = \frac{1}{2}\arctan(2((t_e \pm t_h)/R)$$

Performing the angular average over the field orientation one has

$$\langle I_1\rangle = \frac{(E\mu)^2}{3}\cos^2(\chi)(1+\cos(\beta))$$
$$\langle I_2\rangle = \frac{(E\mu)^2}{3}\sin^2(\chi)(1+\cos(\beta)) \quad \text{(A4)}$$
$$\langle I_3\rangle = \frac{(E\mu)^2}{3}(1-\cos(\beta))$$

The above energy scale is then shifted by adding the LUMO−HOMO energy difference, which is equal to 5.207 eV to fit the position of the TD-DFT results.

Appendix B

Let us consider the problem of evaluating the time-dependent mean value of a given electronic observable, assuming that the system is excited at $t = 0$ by a δ-like pulse, which vertically promotes the ground state wavepacket up to the various PES with a weight dependent on the oscillator strength. With the same geometric assumptions made at the beginning of Appendix A, the vertical excitation from the ground state results in the unnormalized doorway state

$$|d\rangle = c_1|d_1\rangle + c_2|d_2\rangle$$
$$c_1 = \mathbf{E}\cdot\boldsymbol{\mu}_1 = E_0\mu\cos(\theta)$$
$$c_2 = \mathbf{E}\cdot\boldsymbol{\mu}_2 = E_0\mu(\sin(\beta)\sin(\theta)\cos(\phi) + \cos(\beta)\cos(\theta)) \quad \text{(B1)}$$

Here $|d_1\rangle$ and $|d_2\rangle$ are the states obtained by vertical excitation on site 1 and 2, respectively. Hence $|d_1\rangle$, for example, is obtained as a tensor product of the electronic state $|A^*A\rangle$ and the vibrational wavepacket describing the ground vibrational state of the unexcited dimer.

E_0 is the electric filed amplitude and μ the modulus of the adenine transition dipole.

Taking into account that the field is randomly oriented with respect to the dimer, the average of a given observable O is

$$\langle O\rangle_t = \langle d(t)|\hat{O}|d(t)\rangle = a_{11}\langle d_1(t)|\hat{O}|d_1(t)\rangle + a_{22}$$
$$\langle d_2(t)|\hat{O}|d_2(t)\rangle + 2\mathrm{Re}(a_{12}\langle d_1(t)|\hat{O}|d_2(t)\rangle)$$
$$a_{11} = \langle|c_1|^2\rangle_{\mathrm{ang}} = (E_0\mu)^2/3$$
$$a_{22} = \langle|c_2|^2\rangle_{\mathrm{ang}} = (E_0\mu)^2/3$$
$$a_{12} = \langle c_1^* c_2\rangle_{\mathrm{ang}} = \cos(\beta)(E_0\mu)^2/3 \quad \text{(B2)}$$

The above means that we could obtain the average of any observable propagating separately $|d_1\rangle$ and $|d_2\rangle$. For the symmetry of our problem this is, however, not necessary, since we can in principle derive $|d_2(t)\rangle$ from $|d_1(t)\rangle$ by properly exchanging indexes in the MCTDH expansion, eq B1. Unfortunately, due to the approximate nature of the propagation scheme, this approach cannot be pursued. In fact, our MCTDH computations give a very good representation of the vibrational wavepacket on each electronic state as far as the probability distribution is concerned, while the relative phase of wavepackets moving on different PES is much more sensible to numerical errors. This is crucial if one is interested to the population of the various diabatic states. Taking as an example $\hat{O} = \hat{P}_{A^*A} = |A^*A\rangle\langle A^*A|$, eq B2 becomes

$$P_{A^*A}(t) = |\langle d(t)|A^*A\rangle|^2 = \frac{(E_0\mu)^2}{3}(|\langle d_1(t)|A^*A\rangle|^2 +$$
$$|\langle d_2(t)|A^*A\rangle|^2 + 2\cos(\beta)\mathrm{Re}[\langle d_1(t)|A^*A\rangle\langle A^*A|d_2(t)\rangle]) \quad \text{(B3)}$$

Exploiting the symmetry and integrating only on the electronic degrees of freedom one has

$$\langle A^*A|d_2(t)\rangle = \langle AA^*|d_1(t)\rangle = F_{AA^*}(q,Q;t)$$
$$\langle AA^*|d_2(t)\rangle = \langle A^*A|d_1(t)\rangle = F_{A^*A}(q,Q;t) \quad \text{(B4)}$$

where, for example, $F_{A^*A}(q,Q;t)$ is the vibrational wavepacket moving on the $|A^*A\rangle$ PES (the initial state being $|d_1\rangle$).

Equation B3 becomes then

$$P_{A^*A}(t) = \frac{(E_0\mu)^2}{3}(\langle F_{A^*A}|F_{A^*A}\rangle_{\mathrm{nuc}} + \langle F_{AA^*}|F_{AA^*}\rangle_{\mathrm{nuc}} +$$
$$\cos(\beta)\langle F_{A^*A}|F_{AA^*}\rangle_{\mathrm{nuc}}) \quad \text{(B5)}$$

showing that the proper utilization of symmetry arguments is grounded on the possibility of relying on the phase-dependent overlap between vibrational wavepackets moving on different PES.

References and Notes

(1) Crespo-Hernàndez, C. E.; Cohen, B.; Hare, P. M.; Kohler, B. *Chem. Rev.* **2004**, *104*, 1977–2019.
(2) Middleton, C. T.; de La Harpe, K.; Su, C.; Law, Y. K.; Crespo-Hernadez, C. E.; Kohler, B. *Annu. Rev. Phys. Chem.* **2009**, *60*, 13–47.
(3) Schreier, W. J.; Schrader, T. E.; Koller, F. O.; Gilch, P.; Crespo-Hernández, C. E.; Swaminathan, V. N.; Carell, T.; Zinth, W.; Kohler, B. *Science* **2007**, *315*, 625.
(4) Schreier, W. J.; Kubon, J.; Regner, N.; Haiser, K.; Tobias, E.; Schrader, T. E.; Zinth, W.; Clivio, P.; Gilch, P *J. Am. Chem. Soc.* **2009**, *131*, 5038.
(5) Crespo-Hernàndez, C. E.; Cohen, B.; Kohler, B. *Nature* **2005**, *436*, 1141.
(6) Markovitsi, D.; Talbot, F.; Gustavsson, T.; Onidas, D.; Lazzarotto, E.; Marguet, S. *Nature* **2006**, *441*, E7.
(7) Markovitsi, D.; Onidas, D.; Gustavsson, T.; Talbot, F.; Lazzarotto, E. *J. Am. Chem. Soc.* **2005**, *127*, 17130–17131.
(8) Onidas, D.; Gustavsson, T.; Lazzarotto, E.; Markovitsi, D. *J. Phys. Chem. B* **2007**, *111*, 9644–9650.
(9) Schwalb, N.; Temps, F. N. *Science* **2008**, *322*, 243.
(10) Samoylova, E.; Radloff, W.; Hertel, I. V.; Sobolewski, A. L.; Domcke, W. *Science* **2004**, *306*, 1765–1768.
(11) Buchvarov, I.; Wang, Q.; Raytchev, M.; Trifonov, A.; Fiebig, T. *Proc. Natl. Acad. Sci. U.S.A.* **2007**, *104*, 4794–4797.
(12) Tonzani, S.; Schatz, G. C. *J. Am. Chem. Soc.* **2008**, *130*, 7607–7612.
(13) Takaya, T.; Su, C.; de La Harpe, K.; Crespo-Hernàndez, C. E.; Kohler, B. *Proc. Natl. Acad. Sci. U.S.A.* **2008**, *105*, 10285–10290.
(14) Kwok, W.-M.; Ma, C.; Phillips, D. L. *J. Am. Chem. Soc.* **2006**, *128*, 11894–11905.
(15) (a) Serrano-Andres, L.; Merchan, M.; Borin, A. C. *Proc. Nat. Acad. Sci.* **2006**, *103*, 8691–8696. (b) Serrano-Andres, L.; Merchan, M.; Borin, A. C. *Chem.—Eur. J.* **2006**, *12*, 6559. (c) Marian, C. M. *J. Chem. Phys.* **2005**, *122*, 104314.
(16) Karunakaran, V.; Kleinermanns, K.; Improta, R.; Kovalenko, S. A. *J. Am. Chem. Soc.* **2009**, *131*, 5839–5850.
(17) Mercier, Y.; Santoro, F.; Reguero, M. Improta, R. *J. Phys. Chem. B* **2008**, *112*, 10769–10772.
(18) Improta, R.; Barone, V. *Theor. Chem. Acc.* **2008**, *120*, 491–497.
(19) Improta, R.; Barone, V. *J. Am. Chem. Soc.* **2004**, *126*, 14320–14321.
(20) Gustavsson, T.; Banyasz, A.; Lazzarotto, E.; Markovitsi, D.; Scalmani, G.; Frisch, M. J.; Barone, V.; Improta, R. *J. Am. Chem. Soc.* **2006**, *128*, 607–619.
(21) Santoro, F.; Barone, V.; Gustavsson, T.; Improta, R. *J. Am. Chem. Soc.* **2006**, *128*, 16312–16322.
(22) Gustavsson, T.; Sarkar, N.; Lazzarotto, E.; Markovitsi, D.; Barone, V.; Improta, R. *J. Phys. Chem. B* **2006**, *110*, 12843–12847.

(23) Santoro, F.; Barone, V.; Improta, R. *Proc. Nat. Acad. Sci. U.S.A.* **2007**, *104*, 9931–9936.
(24) Improta, R. *Phys. Chem. Chem. Phys.* **2008**, *10*, 2656–2664.
(25) (a) Santoro, F.; Barone, V.; Improta, R. *ChemPhysChem* **2008**, *9*, 2531–2537. (b) Santoro, F.; Barone, V.; Improta, R. *J. Am. Chem. Soc.,* in press.
(26) Lange, A. W.; Rohrdanz, M. A.; Herbert, J. M. *J. Phys. Chem. B* **2008**, *112*, 6304.
(27) Lange, A. W.; Herbert, J. M. *J. Am. Chem. Soc.* **2009**, *131*, 3913–3922.
(28) Olaso-Gonzalez, G.; Merchan, M.; Serrano-Andres, L. *J. Am. Chem. Soc.* **2009**, *131*, 4368–4377.
(29) Eisinger, J.; Guéron, M.; Shulman, R. G.; Yamane, T. *Proc. Natl. Acad. Sci. U.S.A.* **1966**, *55*, 1015–1020.
(30) Bittner, E. R. *J. Chem. Phys.* **2006**, *125*, 094909.
(31) Bittner, E. R. *J. Photochem. Photobiol. A* **2007**, *190*, 328–334.
(32) Tamura, H.; Bittner, E. R.; Burghardt, I. *J. Chem. Phys.* **2007**, *127*, 034706.
(33) Dreuw, A.; Head-Gordon, M. *Chem. Rev.* **2005**, *105*, 4009.
(34) Burke, K.; Werschnik, J.; Gross, E. K. U. *J. Chem. Phys.* **2005**, *123*, 62206.
(35) (a) Adamo, C.; Barone, V. *J. Chem. Phys.* **1999**, *110*, 6158–6170. (b) Ernzerhof, M.; Scuseria, G. E. *J. Chem. Phys.* **1999**, *110*, 5029–5036. (c) Adamo, C.; Scuseria, G. E.; Barone, V. *J. Chem. Phys.* **1999**, *111*, 2889–2899.
(36) (a) Scalmani, G.; Frisch, M. J.; Mennucci, B.; Tomasi, J.; Cammi, R.; Barone, V. *J. Chem. Phys.* **2006**, *124*, 094107. (b) Cossi, M.; Barone, V. *J. Chem. Phys.* **2001**, *115*, 4708–4717.
(37) Barone, V.; Improta, R.; Rega, N. *Acc. Chem. Res.* **2008**, *41*, 605–616.
(38) (a) Improta, R.; Barone, V.; Santoro, F. *Angew Chem., Int. Ed.* **2007**, *46*, 405–408. (b) Improta, R.; Barone, V.; Santoro, F. *J. Phys. Chem. B.* **2007**, *111*, 14080–14082.
(39) (a) Yanai, T.; Tew, D. P.; Handy, N. C. *Chem. Phys. Lett.* **2004**, *393*, 51–55. (b) Tawada, Y.; Tsuneda, T.; Yanagisawa, S.; Yanai, T.; Hirao, K. *J. Chem. Phys.* **2004**, *120*, 8425.
(40) (a) Zhao, Y.; Truhlar, D. G. *Acc. Chem. Res.* **2008**, *41*, 157–167. (b) Zhao, Y.; Schultz, N. E.; Truhlar, D. G. *J. Chem. Theory Comput.* **2006**, *2*, 364.
(41) Vydrov, O. A.; Scuseria, G. E. *J. Chem. Phys.* **2006**, *125*, 234109.
(42) Improta, R.; Scalmani, G.; Frisch, M.; Barone, V. *J. Chem. Phys.* **2007**, *127*, 074504.
(43) Improta, R.; Barone, V.; Scalmani, G.; Frisch, M. J. *J. Chem. Phys.* **2006**, *125*, 054103.
(44) Tomasi, J.; Mennucci, B.; Cammi, R. *Chem. Rev.* **2005**, *105*, 2999.
(45) Frisch, M. J. In *Gaussian03 Development Version*, revision F.02; Gaussian, Inc.: Wallingford, CT, 2007.
(46) (a) Santoro, F.; Improta, R.; Barone, V. *Theor. Chem. Acc.* **2009**, in press. (b) Improta, R.; Barone, V.; Lami, A.; Santoro, F. *J. Phys. Chem. A* **2009**, DOI: 10.1021/jp906524p.
(47) Meyer, H.-D.; Manthe, U.; Cederbaum, L. S. *Chem. Phys. Lett.* **1990**, *171*, 97.
(48) Manthe, U.; Meyer, H.-D.; Cederbaum, L. S. *J. Chem. Phys.* **1992**, *97*, 3193.
(49) Beck, M. H.; Jäckle, A.; Worth, G. A.; Meyer, H.-D. *Phys. Rep.* **2000**, *324*, 1.

JP906278T